GENERATION OF ANGULAR MOMENTUM IN FISSION*

Jørgen Randrup
Lawrence Berkeley National Laboratory, Berkeley, California 94708, USA

Thomas Døssing
Niels Bohr Institutee, University of Copenhagen, Copenhagen 2100, Denmark

Ramona Vogt
Lawrence Livermore National Laboratory, Livermore, California 94551, USA
and
Physics & Astronomy, University of California, Davis, California 95616, USA

Received 19 December 2024, accepted 13 January 2025, published online 10 April 2025

The generation of angular momentum in the primary fission fragments is discussed on the basis of the nucleon exchange transport treatment. Such an analysis leads to the expectation that the wriggling mode (in which the fragments have mutually parallel spins that are perpendicular to the fission direction) is fully populated, while twisting (where the fragments spins are opposite along the fission direction) is unlikely to play a major role; bending (where the fragments have mutually antiparallel spins that are perpendicular to the fission direction) probably has some presence which increases with mass asymmetry and with lower fragment kinetic energies. It is also briefly discussed how measurements of collective E2 photons may reveal the relative presence of the various dinuclear spin modes.

DOI:10.5506/APhysPolBSupp.18.2-A11

1. Introduction

The interest in the generation of angular momentum in fission fragments and in the observational consequences of specific mechanisms is currently intensifying and quite a number of papers on this topic have appeared recently, both theoretical and experimental [1–14].

The present discussion considers particularly the mechanism of nucleon exchange between the two emerging fragments as scission is approached, the mechanism that was found to be of primary importance for damped nuclear reactions [15–19].

* Presented at the 57$^{\text{th}}$ Zakopane Conference on Nuclear Physics, *Extremes of the Nuclear Landscape*, Zakopane, Poland, 25 August–1 September, 2024.

As illustrated in Fig. 1, it should come as no surprise that a fission fragment typically carries about half a dozen units of angular momentum because that is fully consistent with the fact that the intrinsic temperature at scission is about one MeV. The theoretical task is thus to determine the consequences of a particular mechanism for the specific properties of the correlated fragment spin–spin distribution, while the experimental task is to determine those properties.

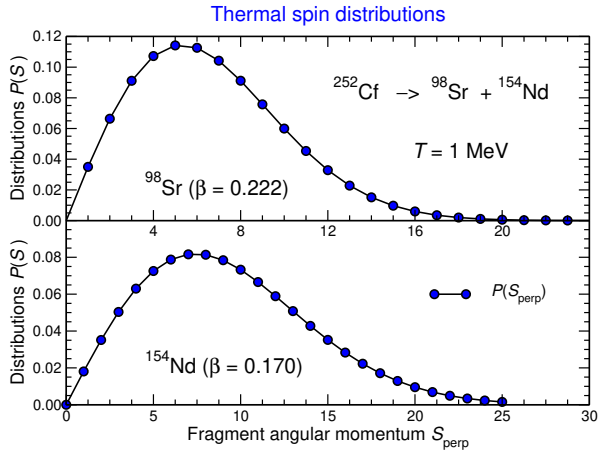

Fig. 1. The distribution of the perpendicular fragment spin $S_\perp$ in equilibrium, $P_A(S_\perp) \sim \exp(-S_\perp^2/2\mathcal{I}_A T)$, for ^{98}Sr and ^{154}Nd, using rigid moments of inertia $\mathcal{I}_A$.

2. Dinuclear rotational modes

As the fissioning system approaches scission, it progressively develops a binary character and eventually it consists of two nascent fragments in close proximity. These carry individual angular momenta, $\boldsymbol{S}_{\rm L(ight)}$ and $\boldsymbol{S}_{\rm H(eavy)}$, their relative motion gives rise to an orbital angular momentum $\boldsymbol{L}$, and the total angular momentum of the system, $\boldsymbol{S}_0 = \boldsymbol{S}_{\rm L} + \boldsymbol{S}_{\rm H} + \boldsymbol{L}$, remains constant throughout the fission evolution.

The six normal modes of internal rotation emerge when the rotational energy, $E_{\rm rot} = S_{\rm L}^2/2\mathcal{I}_{\rm L} + S_{\rm H}^2/2\mathcal{I}_{\rm H} + L^2/2\mathcal{I}_{\rm R}$, is brought onto diagonal form

$$E_{\rm rot} = \frac{S_0^2}{2\mathcal{I}_0} + \frac{s_{\rm wrig}^2}{2\mathcal{I}_{\rm wrig}} + \frac{s_{\rm bend}^2}{2\mathcal{I}_{\rm bend}} + \frac{s_{\rm twst}^2}{2\mathcal{I}_{\rm twst}} + \frac{s_{\rm tilt}^2}{2\mathcal{I}_{\rm tilt}}\,. \tag{1}$$

The six internal modes, denoted *wriggling* ($\boldsymbol{s}_{\rm wrig}$), *bending* ($\boldsymbol{s}_{\rm bend}$), *twisting* ($s_{\rm twst}$), and *tilting* ($s_{\rm tilt}$) [20, 21], carry no net angular momentum and are illustrated in Fig. 2. When none of those are agitated, the system rotates rigidly (the total moment of inertia being $\mathcal{I}_0 = \mathcal{I}_{\rm L} + \mathcal{I}_{\rm H} + \mathcal{I}_{\rm R}$ with $\mathcal{I}_{\rm R} = \mu R^2$).

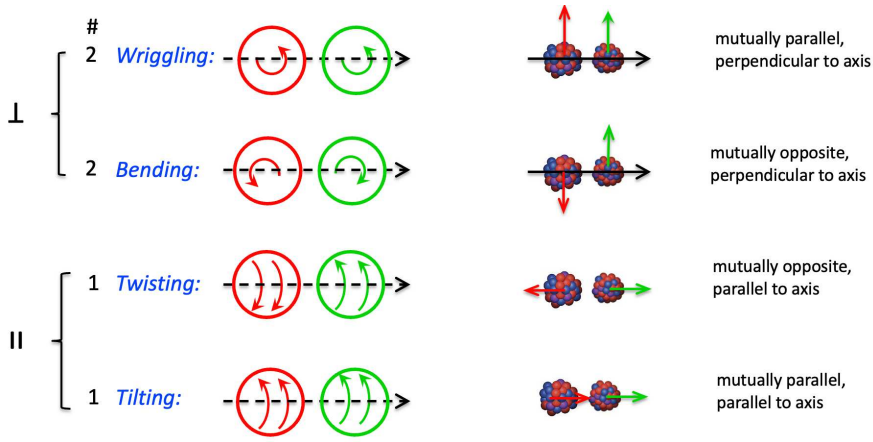

Fig. 2. The six normal modes of internal rotation in the dinuclear complex: the doubly degenerate *wriggling* and *bending* modes have the spins perpendicular to the dinuclear axis and mutually either parallel or opposite, respectively, while the two remaining modes have their spins along the dinuclear axis, being mutually either opposite (*twisting*) or parallel (*tilting*).

The angular momenta of the emerging fragments are thus built up of contributions from the various normal dinuclear rotational modes. The models for fission fragment spins differ in the degree to which those modes are populated, which is reflective of the mechanisms invoked. In thermal equilibrium (first considered by Moretto [21]) the fluctuations associated with mode m have the form $P_m(s_m) \sim \exp(-s_m^2/2\mathcal{I}_m T)$, with the variance of these angular momentum fluctuations being $\langle s_m^2 \rangle_T = \mathcal{I}_m T$.

The normal modes of rotation have the following moments of inertia, $\mathcal{I}_{\rm wrig} = (\mathcal{I}_{\rm L} + \mathcal{I}_{\rm H})\mathcal{I}_{\rm R}/\mathcal{I}_0$, $\mathcal{I}_{\rm bend} = \mathcal{I}_{\rm twst} = \mathcal{I}_{\rm L}\mathcal{I}_{\rm H}/(\mathcal{I}_{\rm L} + \mathcal{I}_{\rm H})$, $\mathcal{I}_{\rm tilt} = \mathcal{I}_{\rm L} + \mathcal{I}_{\rm H}$, and the individual fragment angular momenta $\boldsymbol{S}_{\rm L}$ and $\boldsymbol{S}_{\rm H}$ are given in terms of the normal spins $\boldsymbol{s}_{\rm wrig}$, $\boldsymbol{s}_{\rm bend}$, $s_{\rm twst}$, $s_{\rm tilt}$ as

$$\boldsymbol{S}_{\rm L} = \frac{\mathcal{I}_{\rm L}}{\mathcal{I}_{\rm L} + \mathcal{I}_{\rm H}} \boldsymbol{s}_{\rm wrig} + \boldsymbol{s}_{\rm bend} + (s_{\rm tilt} + s_{\rm twst})\hat{\boldsymbol{R}}, \tag{2}$$

$$\boldsymbol{S}_{\rm H} = \frac{\mathcal{I}_{\rm H}}{\mathcal{I}_{\rm L} + \mathcal{I}_{\rm H}} \boldsymbol{s}_{\rm wrig} - \boldsymbol{s}_{\rm bend} + (s_{\rm tilt} - s_{\rm twst})\hat{\boldsymbol{R}}, \tag{3}$$

where $\hat{\boldsymbol{R}}$ is the direction of the dinuclear axis.

The tilting mode is agitated when the overall dinuclear rotation causes the wriggling rotation to acquire a component along the dinuclear axis and it is thus insignificant in low-energy fission where the overall rotation is slow.

3. Nucleon exchange

Our expectations regarding the agitation of the dinuclear rotational modes may be guided by the Nucleon Exchange Transport model [15, 17]. Although this mechanism was invoked primarily for understanding the dynamical evolution of damped nuclear reactions [16, 18], the basic physics applies equally well to the late stages of fission when the system acquires an ever more prominent binary character.

In this description, individual nucleons are continually being transferred quasi-elastically between the two parts of the dinuclear system, as illustrated in Fig. 3. To a degree depending on the specific nucleonic orbitals involved, each transfer changes the linear and angular momenta of the two parts, as well as their intrinsic excitation energies. As a result, not only the mass and charge partition but also the rotational modes of the system exhibit a diffusive evolution. The net effect on the angular momenta can be expressed in terms of the relaxation times $t_m = \mathcal{I}_m/M_m$, where $\mathcal{I}_m$ is the moment of inertia for the mode and M_m is its mobility coefficient.

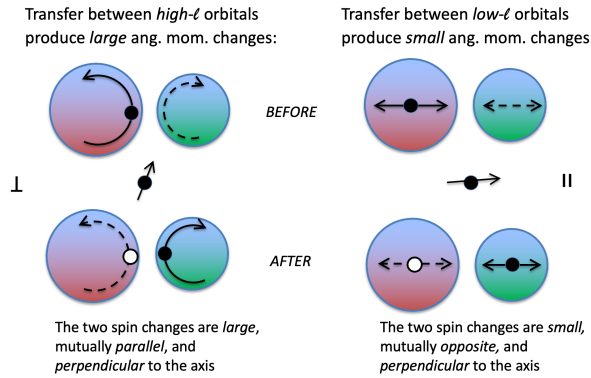

Fig. 3. Schematic illustration of how the transfer of an individual nucleon affects the angular momenta of the two dinuclear partners: When the orbitals involved have high ℓ values (left), the resulting spin changes are large, mutually parallel, and preferentially perpendicular to the dinuclear axis; when the orbitals involved have low ℓ values (right), the resulting spin changes are small, mutually opposite, and preferentially perpendicular to the dinuclear axis.

Expressions for the mobility coefficients were derived in Ref. [19] based on the Nucleon Exchange Transport model presented in Ref. [17]

$$M_{\rm wrig} = m_N \mathcal{N} R^2 \,, \qquad M_{\rm twst} = m_N \mathcal{N} c_{\rm ave}^2 \,, \tag{4}$$

$$M_{\rm bend} = m_N \mathcal{N} \left[\left(\frac{\mathcal{I}_{\rm H} R_{\rm L} - \mathcal{I}_{\rm L} R_{\rm H}}{\mathcal{I}_{\rm L} + \mathcal{I}_{\rm H}} \right)^2 + c_{\rm ave}^2 \right] . \tag{5}$$

Here, m_N is the nucleon mass and the rate of nucleon transfers from one partner to the other is given by $\mathcal{N} \approx \frac{1}{4}\rho\bar{v}\pi c^2$ [22], where ρ is the standard nucleon density, $\bar{v} = \frac{3}{4}v_F$ is the mean nucleon speed, and c is the neck radius. Furthermore, $c^2_{\rm ave} = \frac{1}{2}c^2$ is the average value of c^2. $M_{\rm twst}$ is an order of magnitude smaller than $M_{\rm wrig}$, so $t_{\rm twst} \gg t_{\rm wrig}$. The first term in $M_{\rm bend}$ vanishes for symmetric divisions, giving $M_{\rm bend} = M_{\rm twst}$, but $M_{\rm bend}$ is significantly larger than $M_{\rm twst}$ for typical mass divisions (and small neck radii). These relaxation times are shown in Fig. 4 as functions of c, using $R = R_{\rm L} + R_{\rm H} + d$ with $d = 4$ fm.

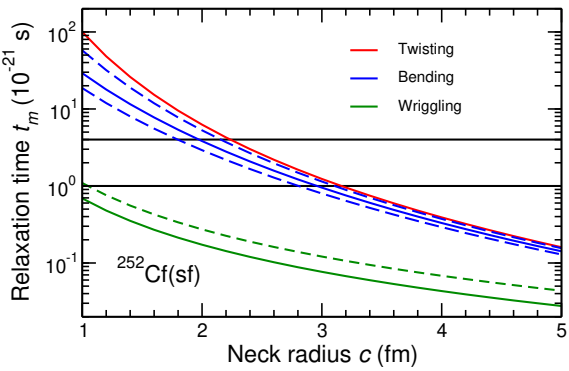

Fig. 4. (Color online) The calculated relaxation times t_m for wriggling (bottom curve, green/light gray), bending (middle three curves, blue/black), and twisting (top curve, red/gray), shown as functions of the neck radius c for a tip separation of $d = 4$ fm. For wriggling there is also shown the result for touching spheres, $d = 0$ (dashed green/light gray). For bending, the solid curve is for the mass division 108:144 (the most probable), while the dashed curves are for 100:152 (lower) and 118:134 (upper) which are each half as probable. Also shown are $t_{\rm fiss} = 1$ zs and $t_{\rm fiss} = 4$ zs (horizontal lines). (From [13].)

In order to put the calculated relaxation times into perspective, they should be compared with $t_{\rm fiss}$, the time it takes the fissioning system to evolve from the first appearance of a dinuclear geometry to the rupture of the neck. This quantity is difficult to measure experimentally and it is not well known [23, 24]. The present discussion assumes that $t_{\rm fiss}$ is in the range of one to several zeptoseconds (1 zs $= 10^{-21}$ s).

The calculated $t_{\rm wrig}$ stays well below the expected range of $t_{\rm fiss}$ and one should therefore expect that the wriggling mode maintains full equilibrium until the time of scission, which is expected to occur for $c \approx 2$ fm.

By contrast, $t_{\rm twst}$ is likely similar to or longer than $t_{\rm fiss}$, so the twisting mode will adjust only slowly as scission is approached. Therefore, for spontaneous fission, where the rotational modes are probably not agitated

much as the system emerges from the tunneling, it may not be possible to build up very much twisting before scission occurs. The situation is more complicated for induced fission. For thermal neutron energies, the local excitation energy in the barrier region is small and even though the system spends a fairly long time there, the low local temperature will limit the degree of agitation of the rotational modes and, consequently, it may not be possible for the twisting mode to adjust to the ever-increasing temperature as scission is approached. But, as the neutron energy is raised, the local temperature in the saddle region increases correspondingly and the twisting mode is more agitated prior to the descent towards scission. Therefore, one should expect an ever-increasing degree of twisting as the impinging neutron energy is raised, an effect that might be observable.

The bending mode is somewhat intermediate and without a more precise estimate of $t_{\rm fiss}$, it is not possible to make specific predictions. But if scission occurs at $c = 2$ fm and $t_{\rm fiss}$ is several times 10^{-21} s, then the bending mode is expected to be agitated to an appreciable degree, though likely not fully. If bending is not fully agitated, wriggling will dominate, and the fragment spins will tend to have parallel directions and their magnitudes will fluctuate in concert. The recent experimental results by Wilson *et al.* [4], suggesting that the spin magnitudes are in fact mutually fairly independent, puts a limit on the possible suppression of the bending mode. It would be very interesting to quantify this by further measurements.

Furthermore, because $t_{\rm bend}$ depends on the mass asymmetry, the degree of bending at scission should increase with the asymmetry. Because the fragment mass is a readily measurable fission observable, this feature is susceptible to experimental investigation as well.

We thus expect the wriggling modes to have reached full equilibrium at scission, while the bending modes may fall somewhat short of that, and though some twisting may be present, it is not likely to play a major role.

Finally, TKE-gated data may also provide valuable information because small TKE values are associated with elongated scission configurations which take more time to reach. Consequently, if the bending mode is only partially equilibrated, it should have a smaller presence in events with large TKE and a larger presence in events with small TKE. This should be reflected, for example, in the degree of correlation between the two fragment spin magnitudes, something that should also be readily measurable.

4. Effect of the post-scission Coulomb force

After scission has occurred, the fission fragments are still interacting via the Coulomb force which exerts a torque on deformed fragments, thereby accelerating their rotations. A particularly simple feature of the Coulomb

spin amplification is that its dependence on the initial spin and the moment of inertia is only through the ratio $S/\mathcal{I}$ and, furthermore, the effect on one fragment is essentially independent of the other.

A recent idealized study [14] has suggested that the effect of the Coulomb torque on the angular momenta of the receding fragments is significant, though not overwhelming, as illustrated in Fig. 5. Therefore, an accurate dynamical treatment of fission should include the effect of the Coulomb force during the post-scission evolution.

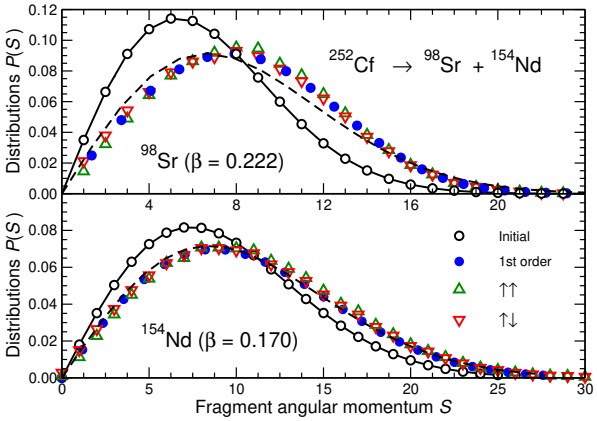

Fig. 5. (Color online) Distributions of pre- and post-Coulomb angular momenta for the fragments ^{98}Sr (top panel) and ^{154}Nd (bottom panel) from the $^{252}\mathrm{Cf} \rightarrow {}^{98}\mathrm{Sr} + {}^{154}\mathrm{Nd}$ reaction, as obtained by either the perturbative calculation (blue solid circles) or by solving the complete coupled equations for 10,000 sampled events as described in [14], with the two fragment spins being either parallel (green triangles pointing up) or anti-parallel (red triangles pointing down). For each of the fragments, the dashed curve is the statistical distribution that has the same *rms* width. The initial statistical distributions of the angular momentum magnitudes, before the action of the Coulomb torque, are indicated by the solid curves with open circles. (From [14].)

However, this presents a delicate challenge because the fragments are distorted away from their equilibrium shapes when released at scission and the resulting Coulomb effect is therefore sensitive to the time scale of the subsequent relaxation of the fragment shapes. In principle, this interplay makes it possible to gain information on the shape relaxation dynamics from the final angular momentum distribution.

5. Observation of fragment angular momentum modes

Important information on the fission fragment angular momenta can be obtained via observation of photons from selected collective E2 transitions.

Being stretched, such transitions preserve the spin alignment and, furthermore, they provide a unique identification of the emitting product nucleus.

5.1. The degree of twisting

The degree to which twisting is populated is reflected in the angular distribution of E2 photons relative to the fragment direction, $\mathrm{d}N_\gamma/\mathrm{d}\theta_{\gamma\mathrm{f}}$,

$$\overline{W}_{\parallel}\left(\theta_{\gamma\mathrm{f}}\right) \;\sim\; 1-\frac{5}{7}P_2\left(\cos\theta_{\gamma\mathrm{f}}\right)-\frac{2}{7}P_4\left(\cos\theta_{\gamma\mathrm{f}}\right)\,, \tag{6}$$

$$\overline{W}_{\perp}\left(\theta_{\gamma\mathrm{f}}\right) \;\sim\; 1+\frac{5}{14}P_2\left(\cos\theta_{\gamma\mathrm{f}}\right)-\frac{3}{28}P_4\left(\cos\theta_{\gamma\mathrm{f}}\right)\,, \tag{7}$$

where the above expressions, which have been averaged over the unobserved photon helicity, hold when the angular momentum is respectively parallel or perpendicular to the fragment velocity, see Fig. 6 (left). By utilizing this feature, it was found that the fragment spins are preferentially perpendicular [25, 26], thus severely limiting the degree of twisting that could be present.

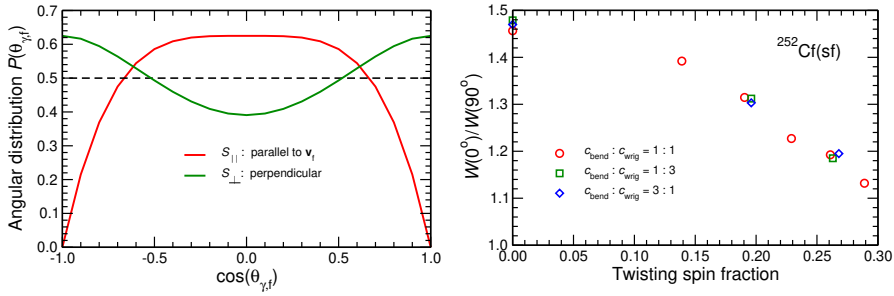

Fig. 6. (Color online) Left: The angular distribution of the collective E2 photons relative to the velocity direction of the emitting product nucleus, $\boldsymbol{V}_\mathrm{f}$, when the product spin is directed either along $\boldsymbol{V}_\mathrm{f}$ (red/light gray) or perpendicular to $\boldsymbol{V}_\mathrm{f}$ (green/black), without any account taken of prior neutron or photon emissions (from [13]). Right: The ratio of the photon yield in the direction of the fragment, $W(0°)$, and the transverse yield, $W(90°)$, as a function of the degree of twisting present at scission, as obtained with FREYA event-by-event simulations. (Adapted from [13].)

Presumably, a quantitative determination of the degree of twisting present could be obtained by repeating such measurements with modern detection equipment. Figure 6 (right) illustrates how the $W(0°):W(90°)$ yield ratio, as obtained from event-by-event simulations with FREYA [27–29], decreases as the presence of twisting is increased, in a manner that is practically insensitive to the relative presence of bending and wriggling [13].

5.2. Bending versus wriggling

The angular distribution of a photon depends on its helicity $h = \pm 1$: Those with $h = +1$ tend to be emitted near the direction of the fragment spin, while those with $h = -1$ tend to be emitted oppositely, as would be intuitively expected. Therefore, provided the helicities can be measured, information about the relative orientation of the two fragment spins could be obtained from photon–photon angular correlations.

In particular, the distribution of the opening angle between (any) two collective photons emitted from a pair of even–even product nuclei would be

$$P^{\pm}(\psi_{12}) = \tfrac{1}{2}P_0(\cos\psi_{12}) \pm \frac{1}{6}h_1h_2P_1(\cos\psi_{12}) + \frac{5}{98}P_2(\cos\psi_{12}) \pm \frac{1}{14}h_1h_2P_3(\cos\psi_{12}) + \frac{2}{441}P_4(\cos\psi_{12}), \quad (8)$$

where $\cos\psi_{12} = \cos\theta_1\cos\theta_2 + \sin\theta_1\sin\theta_2\cos\phi_{12}$ and $\pm$ indicates whether the spins are parallel or anti-parallel. The odd-order terms change sign when the fragment spins change from being parallel to being anti-parallel and the helicity dependence is through the h_1h_2 product. As illustrated in Fig. 7, helicity measurements would thus provide a powerful means for probing the relative direction of the angular momenta of fission fragment partners, information having a crucial bearing on how the spins were generated.

The above example, though beyond our current capabilities, shows the potential utility of helicity measurements for angular-momentum studies and it may thus serve to encourage the required technical developments.

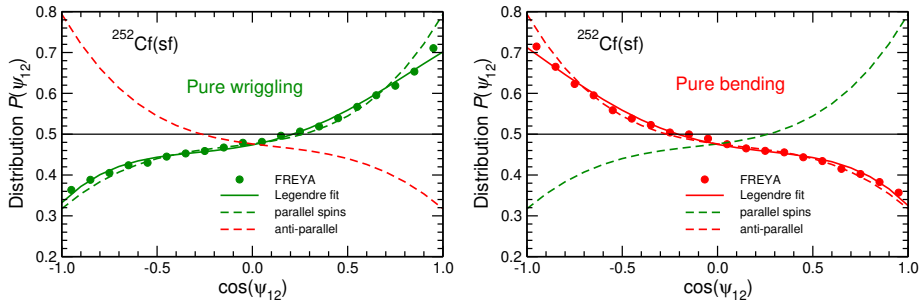

Fig. 7. The distribution of the opening angle ψ_{12} between pairs of collective E2 photons emitted from even–even fission product partners for two extreme scenarios with respect to the dinuclear rotational modes at scission: Only wriggling is present (left) and only bending is present (right). Each panel shows the result of FREYA simulations (dots) and the associated Legendre fit (solid curve), as well as the result of perfectly parallel or anti-parallel fragment spins at the time of emission. Only photon pairs with the same helicity are included; the results for photon pairs having opposite helities would be reflected around $\psi_{12} = 90°$. (Adapted from Ref. [13].)

This work was supported by the Office of Nuclear Physics in the U.S. Department of Energy's Office of Science under Contracts No. DE-AC02-05CH11231 (J.R.) and DE-AC52-07NA27344 (R.V.).

REFERENCES

[1] G.F. Bertsch, T. Kawano, L.M. Robledo, *Phys. Rev. C* **99**, 034603 (2019).
[2] A. Al-Adili *et al.*, *EPJ Web Conf.* **256**, 00002 (2021).
[3] M. Travar *et al.*, *Phys. Lett. B* **817**, 136293 (2021).
[4] J. Wilson *et al.*, *Nature (London)* **590**, 566 (2021).
[5] R. Vogt, J. Randrup, *Phys. Rev. C* **103**, 014610 (2021).
[6] A. Bulgac *et al.*, *Phys. Rev. Lett.* **126**, 142502 (2021).
[7] P. Marević, N. Schunck, J. Randrup, R. Vogt, *Phys. Rev. C* **104**, L021601 (2021).
[8] J. Randrup, R. Vogt, *Phys. Rev. Lett.* **127**, 062502 (2021).
[9] S. Marin *et al.*, *Phys. Rev. C* **104**, 024602 (2021).
[10] I. Stetcu *et al.*, *Phys. Rev. Lett.* **127**, 222502 (2021).
[11] S. Marin *et al.*, *Phys. Rev. C* **105**, 054609 (2022).
[12] A. Bulgac, I. Abdurrahman, K. Godbey, I. Stetcu, *Phys. Rev. Lett.* **128**, 022501 (2022).
[13] J. Randrup, T. Døssing, R. Vogt, *Phys. Rev. C* **106**, 014609 (2022).
[14] J. Randrup, *Phys. Rev. C* **108**, 064606 (2023).
[15] J. Randrup, *Nucl. Phys. A* **327**, 490 (1979).
[16] W.U. Schröder *et al.*, *Phys. Rev. Lett.* **44**, 308 (1980).
[17] J. Randrup, *Nucl. Phys. A* **383**, 468 (1982).
[18] W.U. Schröder, J.P. Huizenga, in: D.A. Bromley (Ed.) «Treatise on Heavy-Ion Science», *Plenum*, New York 1984, p. 115.
[19] T. Døssing, J. Randrup, *Nucl. Phys. A* **433**, 215 (1985).
[20] J.R. Nix, W.J. Swiatecki, *Nucl. Phys.* **71**, 1 (1965).
[21] L.G. Moretto, R.P. Schmitt, *Phys. Rev. C* **21**, 204 (1980).
[22] J. Błocki *et al.*, *Ann. Phys.* **113**, 330 (1978).
[23] B.B. Back, in: J. Hamilton (Ed.) «Proceedings of the Sixth International Conference on Fission and Neutron-Rich Nuclei», *World Scientific*, Singapore 2017, p. 600.
[24] B.B. Back, *JPS Conf. Proc.* **32**, 010002 (2020).
[25] J.B. Wilhelmy *et al.*, *Phys. Rev. C* **5**, 2041 (1972).
[26] A. Wolf, E. Cheifetz, *Phys. Rev. C* **13**, 1952 (1976).
[27] J.M. Verbeke, J. Randrup, R. Vogt, *Comput. Phys. Commun.* **191**, 178 (2015).
[28] J. Randrup, R.Vogt, *Phys. Rev. C* **89**, 044601 (2014).
[29] J.M. Verbeke, J. Randrup, R. Vogt, *Comput. Phys. Commun.* **222**, 263 (2018).